A Model of Redox Kinetics Implicates the Thiol Proteome in Cellular Hydrogen Peroxide Responses

3 authors, including:

Dean Jones
Emory University
750 PUBLICATIONS   **36,613** CITATIONS

SEE PROFILE

Melissa Kemp
Georgia Institute of Technology
121 PUBLICATIONS   **1,080** CITATIONS

SEE PROFILE

Some of the authors of this publication are also working on these related projects:

Create new project "Predictive Health, Center for Health Discovery and Well Being" View project

An Environment-wide Association Study in Autism Spectrum Disorders Using Novel Bioinformatics Methods and Metabolomics via Mass Spectrometry View project

ORIGINAL RESEARCH COMMUNICATION

A Model of Redox Kinetics Implicates the Thiol Proteome in Cellular Hydrogen Peroxide Responses

Nnenna J. Adimora,[1] Dean P. Jones,[2] and Melissa L. Kemp[1]

Abstract

Hydrogen peroxide is appreciated as a cellular signaling molecule with second-messenger properties, yet the mechanisms by which the cell protects against intracellular H_2O_2 accumulation are not fully understood. We introduce a network model of H_2O_2 clearance that includes the pseudo-enzymatic oxidative turnover of protein thiols, the enzymatic actions of catalase, glutathione peroxidase, peroxiredoxin, and glutaredoxin, and the redox reactions of thioredoxin and glutathione. Simulations reproduced experimental observations of the rapid and transient oxidation of glutathione and the rapid, sustained oxidation of thioredoxin on exposure to extracellular H_2O_2. The model correctly predicted early oxidation profiles for the glutathione and thioredoxin redox couples across a range of initial extracellular $[H_2O_2]$ and highlights the importance of cytoplasmic membrane permeability to the cellular defense against exogenous sources of H_2O_2. The protein oxidation profile predicted by the model suggests that approximately 10% of intracellular protein thiols react with hydrogen peroxide at substantial rates, with a majority of these proteins forming protein disulfides as opposed to protein S-glutathionylated adducts. A steady-state flux analysis predicted an unequal distribution of the intracellular anti-oxidative burden between thioredoxin-dependent and glutathione-dependent antioxidant pathways, with the former contributing the majority of the cellular antioxidant defense due to peroxiredoxins and protein disulfides. *Antioxid. Redox Signal.* 13, 731–743.

Introduction

AN ACCUMULATION of reactive oxygen species within the cell can lead to oxidative stress, resulting in changes in the redox state of many proteins (46). Although cellular processes such as growth, proliferation and apoptosis are controlled by the overall redox state of the cell (41), high levels of ROS can be toxic (24, 42). The oxidant hydrogen peroxide (H_2O_2) is of great interest to researchers because it is continuously produced as a result of cellular metabolism, diffuses across cellular membranes, has a longer half-life than other oxidative species, and reversibly oxidizes protein thiols (3, 9, 24).

The apparent paradox between the role of H_2O_2 as a cellular signaling molecule and its role as a cellular toxin appears to be highly dependent on its intracellular concentration, and the resolution of several key questions regarding how mammalian cells handle peroxide levels will facilitate our understanding of this paradox: Which antioxidant mechanisms exert the most control over the removal of hydrogen peroxide from the cell, and how could this be affected by intervention?

How independent are the redox couples from one another during oxidative stress? What role does the global protein thiol pool play in antioxidant defense? To address these questions accurately, quantitative computational modeling that integrates the known mechanisms by which mammalian cells control intracellular H_2O_2 accumulation during periods of oxidative stress is necessary. This form of analysis addresses whether our current knowledge can quantitatively account for observed cellular behavior. Ultimately, modeling can provide additional insight into the discrimination of the physiologic function of H_2O_2 from its pathologic role.

Researchers have a general understanding of the key players involved in a cell's ability to maintain its intracellular redox state, and most models of H_2O_2 depletion can accurately describe one or two aspects of this system (3, 28, 40, 42). A previous mathematical model developed by Antunes and Cadenas (3), for example, offered great insight into the enzymatic contributions of glutathione peroxidase (GPx) and catalase to the development of peroxide gradients across cellular membranes. Antunes' model provided a new quantitative estimate for the H_2O_2 membrane permeability coefficient,

[1]Wallace H. Coulter Department of Biomedical Engineering, Georgia Institute of Technology and Emory University, Atlanta, Georgia.
[2]Emory University Department of Medicine, Division of Pulmonary Medicine, Atlanta, Georgia.

one that was an order of magnitude smaller than that cited in the literature (28, 42). Although Antunes' model provided novel findings, the model did not consider the enzymatic contribution of peroxiredoxins and the nonenzymatic contribution of protein thiols. Since the publication of Antunes' model, multiple studies have revealed that the previously accepted reaction rate of peroxiredoxin with H_2O_2 grossly underestimated its true value (29, 37). Increased rates of H_2O_2 consumption, therefore, may suggest an H_2O_2 permeability coefficient that is even smaller than that predicted by Antunes and co-workers. As researchers gain a more thorough understanding of the different components that play a role in intracellular H_2O_2 consumption, the accepted kinetic reactions rates of particular species with H_2O_2 will have to be amended.

Over the past few years, our knowledge of the varied intracellular antioxidant systems has increased, and the need for a comprehensive model that incorporates these new findings is evident. The highly complex nature of the system in question, which results from the interconnectivity between protein thiol oxidation and redox couples during transient oxidative stress, has made development of integrative models difficult. For instance, the antioxidative roles of glutathione peroxidase (GPx) and peroxiredoxins (Prxs) depend directly on the reducing capacities of their respective co-substrate molecules, glutathione (GSH) and thioredoxin (Trx). To maintain their reducing capacities, GSH and Trx depend on the enzymes glutathione reductase (GR) and thioredoxin reductase (TR), respectively, in addition to NADPH. Moreover, the codependence of both the GSH and Trx thiol/disulfide redox couples on NADPH regeneration does not readily explain their maintenance at dissimilar nonequilibrium redox potentials (20, 21).

We have generated a network model of major redox reactions and cellular thiol modifications involved in H_2O_2 metabolism to improve our understanding of the processes by which a cell deals with H_2O_2-induced oxidative stress. Before we continue, however, we must clarify the term "buffering" as it applies to the redox systems that are described. Here, the term buffering is not used to describe a system at equilibrium; rather, it is used to describe the process by which the intracellular redox network, as a whole, protects against deviations in the redox states of the individual components that make up the network. This model, therefore, takes into account not only the key components of the network, but also the hierarchic interdependence of each component on the other. It builds in scope on prior modeling studies (3, 28, 40, 42) to explore the collective features of an intact redox system by accounting for all the major enzymes known to consume hydrogen peroxide in the cytosol, as well as the pseudo-enzymatic oxidative turnover of protein thiols. The use of computational modeling to study peroxide buffering allows a detailed investigation of the cellular dynamics of oxidative stress.

Computational Methods

Overview of model structure

We developed a computational model, based on ordinary differential equations, by using mass action and Michaelis-Menten kinetics to describe the changes in concentration of cellular redox-buffering components on exposure to extra-

cellular H_2O_2. Figure 1 is an illustration of the reactions included in the model. Organellar compartmentation provides additional regulatory control in redox mechanisms by maintenance of nonequilibrium redox potentials (14); this present model was simplified in description to the extracellular medium, intracellular cytosol, and the peroxisomes. Intracellular generation of hydrogen peroxide by the mitochondria was described by a zero-order production term, and the more rapid oxidation rate of Trx2 (14) was excluded from the model.

In this model, the antioxidative capacity of the cell was divided into several branches, with each branch describing a particular mode of H_2O_2 elimination. The first branch described H_2O_2 elimination by the catalase enzyme. An average of two peroxisomes per cell has been measured in Jurkat cells (17), and all the catalase activity within the cell was assumed to occur inside the peroxisomes.

The second branch of H_2O_2 elimination described the glutathione peroxidase enzymes (GPx). Although multiple GPx isozymes are present in cells, and some glutathione S-transferases have GPx activity, a reliable value for the cytosolic concentration of GPx in Jurkat cells is unknown (3). For the purpose of modeling this system, we simplified this description by considering the predominant glutathione peroxidase, GPx1, and implemented the literature-reported estimate of the intracellular concentration of GPx as predicted by a previous generalized mathematical model (33). GPx catalyzes the reaction of hydrogen peroxide with GSH to produce glutathione disulfide (GSSG). Glutathione disulfide is subsequently reduced through the actions of GR and NADPH (3, 28).

The third branch of H_2O_2 elimination accounted for the peroxiredoxin (Prx) enzymes in conjunction with Trx, TR, and NADPH. Mammalian cells have several members of the peroxiredoxin family, but the predominant mammalian cytoplasmic Prxs are peroxiredoxin 1 and 2 (31, 37); the combined contributions of these two isoforms were described in the model. The total concentration of cytosolic Prx in Jurkat cells was estimated from the literature (6, 31). The total concentrations of reduced and oxidized NADPH were estimated from values reported in the literature (30, 41). Cytosolic Trx1, at a concentration of 0.5 μM (48), was distributed between its reduced and oxidized forms, as experimentally determined for this study by redox Western blot.

The fourth branch of H_2O_2 elimination involved the oxidation of cysteine residues of intracellular proteins (Pr-SH/Pr-$(SH)_2$). Cysteine (Cys) residues of intracellular proteins contain redox-sensitive thiols that are susceptible to oxidation (46). On oxidation, the Cys residues of proteins can be reduced, with different characteristics, depending on the microenvironment, through a system of reactions involving GSH or Trx (9, 36, 46); vicinal dithiols are considered to form protein disulfides (P-SS-P) that are reduced by Trx1. Other thiols are oxidized to protein sulfenic acids (P-SOH), which undergo protein S-glutathionylation (P-SSG). The model reserved protein disulfide reduction exclusively for Trx, whereas protein sulfenic acids were reduced exclusively by GSH-dependent reactions (Fig. 1) (9). Methionine residues are also subject to oxidation, but the rates are not known. Because methionine sulfoxide reductases are thioredoxin dependent, the model, as described, can be considered to have methionine oxidation grouped with Trx-dependent reductions (19).
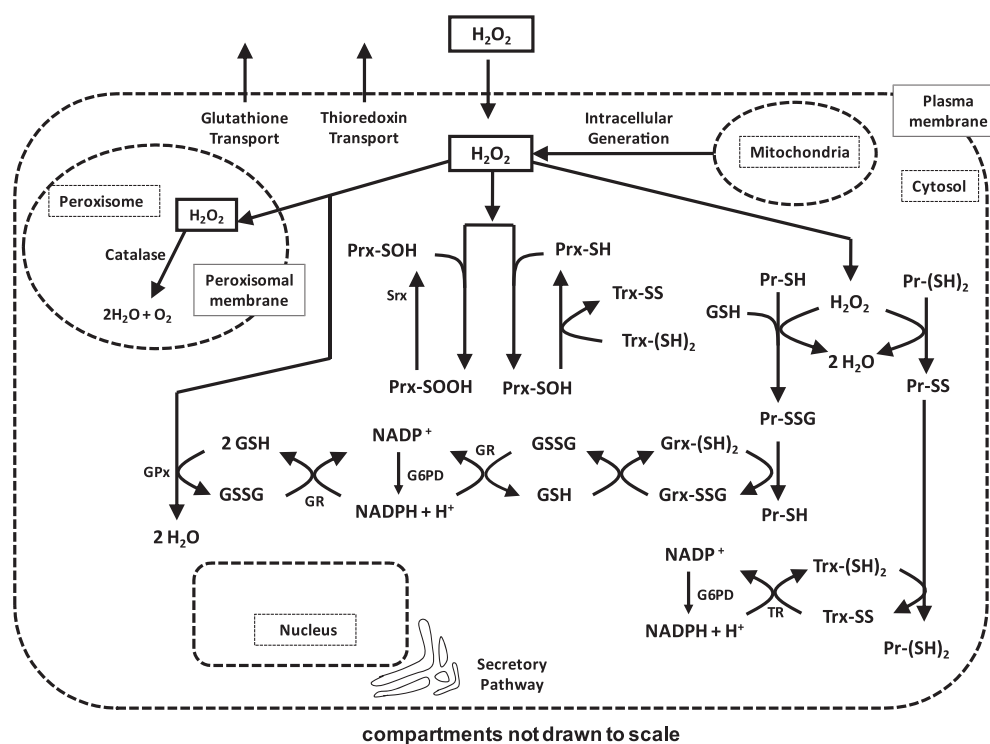
FIG. 1. Model of hydrogen peroxide (H_2O_2) elimination by Jurkat T cells. The modeled system was that of an individual cell with three compartments being considered: the extracellular medium, the intracellular cytosol, and the peroxisomes. H_2O_2 freely moved between compartments by permeating through the cytoplasmic and peroxisomal membranes. A constant intracellular H_2O_2 production rate was defined with a mitochondrial source. Within the intracellular cytosol, H_2O_2 was metabolized by a series of reactions (*arrows*), each with a given reaction-rate constant (Table 1). By four main pathways, H_2O_2 was metabolized by the cell. The first was controlled by catalase, and the second was controlled by glutathione peroxidase (GPx) enzymes working in conjunction with GSH, GR, and NADPH. The third was controlled by the peroxiredoxin enzymes (Prx) working in conjunction with Trx, TR, and NADPH. The fourth and final pathway described the nonenzymatic elimination of H_2O_2 through the oxidation of cysteine residues on intracellular proteins. This can occur at single Cys residues, resulting in sulfenic acids, which react with GSH to form glutathionylated intermediates. Alternatively, this can occur at dithiols resulting in the formation of an internal disulfide.

Parameter and species fitting

For this global model that encompassed 28 kinetic parameters and 24 species, some several values had yet to be appropriately defined in the literature: the H_2O_2 permeability constant, the rate of protein thiol oxidation, and the concentration of protein thiols dependent on GSH and Trx1, respectively, for reduction (Tables 1 and 2). Experimentally determined dynamics, therefore, were used for model fitting to arrive at acceptable estimates for these parameters and species (Fig. 2). The first experimental data set used for parameter fitting was digitized from the results of Antunes and Cadenas (3) describing the consumption of a bolus addition of extracellular H_2O_2 by intact Jurkat cells (Fig. 2B). Four additional data sets were generated under identical experimental conditions and quantified by using HPLC techniques and redox Western blots. These results described the changes in distribution of GSH and GSSG, as well as reduced and oxidized cytosolic Trx1, that occur as a result of H_2O_2 treatment (Fig. 2C and D). Parameters were estimated by minimizing an objective function, comprising the normalized root mean square deviation (RMSD) between experimentally observed time-course data and computed model predictions (8).

Two models of protein oxidation

Accurate modeling of the contribution of protein thiols to the overall redox network requires both the known values of the protein thiol concentration susceptible to reacting with hydrogen peroxide and the rates at which these reactions occur. We postulated two distinct models of protein thiol oxidation to determine the proper description of protein oxidation, a "slow" model and a "fast" model, and tested the ability of each model to match the experimental data (Fig. 2). The slow model was constructed by assuming the total available protein thiol pool, as estimated by Jones (19), reacted with intracellular hydrogen peroxide with the preestablished rate constant of 5×10^2 M/s, the rate at which GAPDH is estimated to react with hydrogen peroxide (49). In this model, the available protein thiol pool was further divided into two subgroups: the protein monothiol pool (Pr-SH), which contained 50% of the total available protein thiols, and the protein dithiol pool (Pr-(SH)$_2$), which contained the remaining 50% of the total protein thiol pool (Fig. 2A, left panel). The fast model, conversely, was constructed by assuming that a smaller subset of protein thiols existed, approximately 20% of the total available protein thiol pool, which reacted with hydrogen peroxide at an appreciably faster rate than that estimated for

TABLE 1. MODEL PARAMETERS

Rxn No.	Expression	Parameter	Reference
R_1	$k_1 ([H_2O_2]_{media}) (A)^a$	$k_1 = 1.0 \times 10^{-5} \, cm/s$	Fitted
R_2	H_2O_2 intracellular generation	$k_2 = 1.1 \times 10^{-7} \, M/s$	(19)
R_3	$k_3 ([H_2O_2]_{cytosol}) ([GPx_{red}])$	$k_3 = 2.1 \times 10^7 \, M^{-1} s^{-1}$	(33)
R_4	$k_4 ([GSH]) ([GPx_{ox}])$	$k_4 = 4 \times 10^4 \, M^{-1} s^{-1}$	(33)
R_5	$k_5 ([GSH]) ([GPx\text{-}SSG])$	$k_5 = 1 \times 10^7 \, M^{-1} s^{-1}$	(33)
R_6	$k_6 ([H_2O_2]_{cytosol}) ([Catalase])$	$k_6 = 3.4 \times 10^7 \, M^{-1} s^{-1}$	(1, 37)
R_7	$k_{22} ([NADP^+] - [NADP^+]_i)/(k_7 + [NADP^+])$	$k_7 = 5.7 \times 10^{-5} \, M$	(52)
R_8	$k_8 ([H_2O_2]_{cytosol}) ([Prx\text{-}(SH)_2])$	$k_8 = 4 \times 10^7 \, M^{-1} s^{-1}$	(49)
R_9	$k_9 ([H_2O_2]_{cytosol}) ([Prx\text{-}SOH])$	$k_9 = 7.2 \times 10^4 \, M^{-1} s^{-1}$	(51)
R_{10}	$k_{10} ([Prx\text{-}SO_2H])$	$k_{10} = 3 \times 10^{-3} \, per \, s$	(7)
R_{11}	$k_{11} ([Prx\text{-}SOH])$	$k_{11} = 15 \, per \, s$	(44)
R_{12}	$k_{12} ([Prx\text{-}SS]) ([Trx_{red}])$	$k_{12} = 2.1 \times 10^6 \, M^{-1} s^{-1}$	(26)
R_{13}	$k_{13} ([GSH]) ([GSH])$	$k_{13} = 7.4 \times 10^{-5} \, per \, s$	(40)
R_{14}	$k_{14} ([Pr\text{-}(SH)]) ([H_2O_2]_{cytosol})$	$k_{14} = 1 \times 10^4 \, M^{-1} s^{-1}$	Fitted
R_{15}	$k_{15} ([GSH]) ([Pr\text{-}SOH] - [Pr\text{-}SOH]_i)$	$k_{15} = 1.2 \times 10^5 \, M^{-1} s^{-1}$	(11, 25)
R_{16}	$k_{16} ([Grx\text{-}SH]) ([Pr\text{-}SSG] - [Pr\text{-}SSG]_i)$	$k_{16} = 9.1 \times 10^4 \, M^{-1} s^{-1}$	(36)
R_{17}	$k_{17} ([Grx\text{-}SSG] - [Grx\text{-}SSG]_i) ([GSH])$	$k_{17} = 3.7 \times 10^4 \, M^{-1} s^{-1}$	(43)
R_{18}	$k_{18} ([Pr\text{-}(SH)_2]) ([H_2O_2]_{cytosol})$	$k_{18} = 5 \times 10^5 \, M^{-1} s^{-1}$	Fitted
R_{19}	$k_{19} ([Trx_{red}]) ([Pr\text{-}SS] - [Pr\text{-}SS]_i)$	$k_{19} = 1 \times 10^5 \, M^{-1} s^{-1}$	(16)
R_{20}	$k_{20} ([GSSG] - [GSSG]_i) ([NADPH])$	$k_{20} = 3.2 \times 10^6 \, M^{-1} s^{-1}$	(15)
R_{21}	$k_{21} ([Trx_{ox}] - [Trx_{ox}]_i) ([NADPH])$	$k_{21} = 2 \times 10^7 \, M^{-1} s^{-1}$	(4)
R_{22}	$k_{22} ([NADP^+] - [NADP^+]_i)/(k_7 + [NADP^+])$	$k_{22} = 3.75 \times 10^{-4} \, M/s$	(52)
R_{23}	$k_{23}([H_2O_2]_{cytosol})(B)^b$	$k_{23} = 3 \times 10^{-3} \, cm \, s^{-1}$	(38)
R_{24}	GSH synthesis	$k_{24} = 4.1 \times 10^{-7} \, M/s$	(21)
R_{25}	GSSG efflux	$k_{25} = 1.2 \times 10^{-8} \, M/s$	(2)
R_{26}	GSH + GSSG efflux	$k_{26} = 1.2 \times 10^{-7} \, M/s$	(23)
R_{27}	Trx efflux	$k_{27} = 7.5 \times 10^{-10} \, M/s$	(22)
R_{28}	Trx synthesis	$k_{28} = 7.0 \times 10^{-10} \, M/s$	(22)

[a] $A = 10^{-3} \, (L \, cm^{-3}) \times 6.5 \times 10^{-5} \, (cm^2) \times 1 \times 10^9 \, (cells/L)$.
[b] $B = 10^{-3} \, (L \, cm^{-3}) \times 3.0 \times 10^{-9} \, (cm^2) \times 1.5 \times 10^{14} \, (L^{-1})$.

TABLE 2. SPECIES INITIAL CONCENTRATIONS

Species	Initial condition (M)	Reference
$[H_2O_2]_{media}$	1×10^{-4}	Assigned
$[H_2O_2]_{cytosol}$	1×10^{-9}	(35)
$[GPx_{red}]$	5×10^{-5}	(33)
$[GPx_{ox}]$	1×10^{-14} [a]	Assigned
$[GPx\text{-}SSG]$	1×10^{-14} [a]	Assigned
$[GSH]$	3.68×10^{-4}	Measured
$[GSSG]$	1.78×10^{-6}	Measured
$[Catalase]$	9×10^{-7}	(32, 38)
$[H_2O_2]_{peroxisome}$	1×10^{-10} [a]	Assigned
$[Prx\text{-}(SH)_2]$	1.9×10^{-5}	(14, 39)
$[Prx\text{-}(SOH)]$	1×10^{-14} [a]	Assigned
$[Prx\text{-}(SOOH)]$	1×10^{-14} [a]	Assigned
$[Prx\text{-}SS]$	9.6×10^{-8} [b]	(19)
$[Trx_{red}]$	4.3×10^{-7}	Measured
$[Trx_{ox}]$	7.5×10^{-8}	Measured
$[Pr\text{-}SH]$	1.22×10^{-4}	Fitted
$[Pr\text{-}SOH]$	6.1×10^{-7} [b]	(19)
$[Pr\text{-}SSG]$	6.1×10^{-7} [b]	(19)
$[Grx\text{-}SH]$	1.2×10^{-6}	(27)
$[Grx\text{-}SSG]$	6.0×10^{-9} [b]	(19)
$[Pr\text{-}(SH)_2]$	1.0×10^{-3}	Fitted
$[Pr\text{-}(SS)]$	5.5×10^{-6} [b]	(19)
$[NADPH]$	3.0×10^{-5}	(30)
$[NADP^+]$	3.0×10^{-7}	(41)

[a] Baseline assignment to highlight the effects of exogenously applied H_2O_2 only.
[b] Estimate of 0.5% [protein] in the glutathionylated form (19).

GAPDH oxidation. The remaining 80% of the total protein thiol pool was divided equally between the protein monothiol group and the protein dithiol group and was allowed to react with hydrogen peroxide at the slower rate constant of $5 \times 10^2 \, M/s$. The purpose of the fast model was to determine the percentage of the highly reactive protein thiols that belonged to the protein monothiol group and the protein dithiol group, respectively, and to predict the rates of reactions of these fast-reacting thiols with intracellular hydrogen peroxide (Fig. 2A, right panel).

Parameter estimation

The parameters predicted by the model were (a) the concentration of fast-reacting protein monothiols [Pr-(SH)], (b) the reaction rate constant for the fast-reacting protein monothiols with hydrogen peroxide, (c) the concentration of fast-reacting protein dithiols (Pr-(SH)₂), (d) the reaction rate constant for the fast-reacting protein dithiols with hydrogen peroxide, and (e) the permeability coefficient of the cytoplasmic membrane. The protein oxidation parameters to be fitted were initialized to randomized values that lay within the literature-reported estimates of their upper and lower bounds (9, 49, 50). Because of conflicting estimates of the lower bound of the permeability coefficient (3, 28, 42), it was deemed appropriate to expand the lower bound of the explored parameter space for this parameter by one order of magnitude. Multiple simulations were conducted for each condition ($n = 2,000$ runs), in which each of the three un-
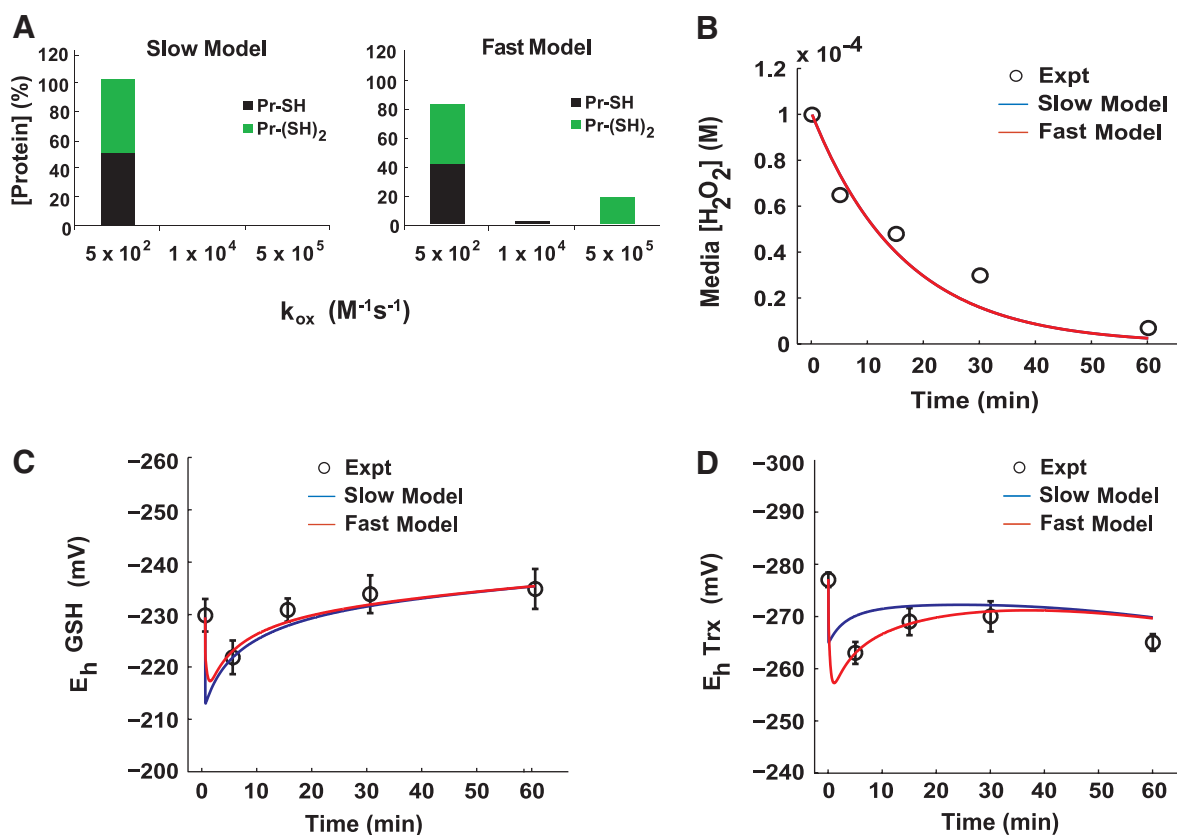
FIG. 2. A model with rapid protein dithiol oxidation accurately describes hydrogen peroxide consumption. (**A**) Assignment of the distribution of protein thiol pools and rate constants for the slow and fast protein thiol oxidation models. (**B**) Experimental data (3) and model fitted results for the slow and fast protein thiol oxidation models showing the consumption of H_2O_2 by intact Jurkat T cells at a density of a 1×10^6 cells/ml after being exposed to a bolus addition of $100 \, \mu M$ extracellular H_2O_2. (**C**) Redox states of the glutathione redox couple as experimentally determined and model fitted for the slow and fast models. Experimental values represent the mean $\pm$ SEM of three separate experiments. (**D**) Redox states of the thioredoxin redox couple as experimentally determined and model fitted for the slow and fast protein thiol oxidation models. Experimental values represent the mean $\pm$ SEM of three separate experiments.

known parameters was simultaneously assigned a random initial value from its allowable parameter space and the objective function calculated. The parameter set that resulted in the minimization of the objective function was selected as the optimal model description.

Membrane H_2O_2 transport

The rate of movement of H_2O_2 across the cytoplasmic membrane was described previously by the following (42):

$$\frac{d[H_2O_2]_{media}}{dt} = - \left([H_2O_2]_{cytosol} - [H_2O_2]_{media} \right) \\ \times 10^{-3} \left(\frac{L}{cm^3} \right) \times P \left(\frac{cm}{s} \right) \times A \left(cm^2 \right) \times \frac{cells}{L} \quad (1)$$

where $[H_2O_2]_{media}$ and $[H_2O_2]_{cytosol}$ represent the concentration of peroxide in the extracellular media and the intracellular cytosol, respectively, at time t. H_2O_2 flux across the cytoplasmic membrane was a function of the intra- and extracellular concentration of H_2O_2, the permeability coefficient of H_2O_2 through the cytoplasmic membrane, P, and the surface area of the cell, A, approximately $1.0 \times 10^{-5} \, cm^2$, as calculated from the average diameter of the Jurkat cell, $20 \, \mu m$

(ViCell Viability Counter, Beckman Coulter). The volume of the cytoplasmic compartment was calculated by assuming the Jurkat cell to be a perfect sphere. The concentration of H_2O_2 in a cell was described previously as a sum of the influx, production, efflux, and scavenging of H_2O_2 within a particular cellular compartment (5). H_2O_2 flux across the peroxisomal membrane was modeled in a similar fashion by using the concentration of peroxide in the cytosol and the concentration of peroxide in the peroxisome to generate the gradient force for diffusion. The permeability coefficient of H_2O_2 through the peroxisomal membrane, P, was obtained from the literature (38), assuming a uniform concentration of H_2O_2 within a particular compartment.

Parameter values

The majority of the rate constants and initial species concentrations used in this model were derived from published data (Tables 1 and 2, respectively). Where possible, values reported specifically for Jurkat cells were used; reactions and species exist, however, for which Jurkat cell line–specific values were undefined. For these types of reactions, we used published data for other cell lines as an appropriate estimate. The fractional cytosolic volume used for concentration

calculations was defined as 30% of total cell volume by estimation from images of Hoescht nuclear-stained Jurkat cells.

Description of reaction kinetics

The series of differential equations was solved by using Matlab R2008a (Mathworks, Natick, MA). The generalized equation for a particular species constituted the sum of all reactions that produced the species minus the sum of all reactions that consumed it. Several components in the model, however, deviated from the generalized equation form, as described later.

Ideally, if the law of mass action were used to describe the reduction of GSSG by GR to produce GSH, the resulting equations would resemble the following:

$$GSSG + NADPH + H^+ \rightarrow 2GSH + NADP^+ \tag{2}$$
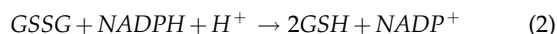
$$\frac{d[GSH]}{dt} = 2 \times k_{20} \times [GSSG] \times [NADPH] \times [H^+] \tag{3}$$

where [GSH], [GSSG], and [NADPH] represented the intracellular concentrations of reduced glutathione, glutathione disulfide, and NADPH, respectively, at time t, and k_{20} represented the rate constant for the reduction reaction. Instead of Equation 3, the change in concentration of GSH as a result of the reduction of GSSG by GR was described in the model by the following:

$$\frac{d[GSH]}{dt} = 2 \times k_{20} \times ([GSSG] - [GSSG]_i) \times [NADPH] \tag{4}$$

where [GSSG]$_i$ represented the initial concentration of glutathione disulfide in the cell. Because the cell maintains a fixed nonequilibrium ratio of [GSH] to [GSSG] under normal oxidative conditions (21), the spontaneous reduction of GSSG in the absence of oxidants could not be allowed. To prevent this behavior, the reduction of GSSG was modeled as a function of the difference between [GSSG] and [GSSG]$_i$. Although this model correctly captured any oxidant-induced changes to this reduction rate, the absolute GSSG reduction rate in the model may be somewhat underestimated by the endogenous rate at baseline, because the K_m of GR is high relative to concentrations of GSSG achieved in cells (12). The same basic principles and assumptions also have been applied to the reactions involving the Trx redox couple. The rate expressions governing the change in concentration of each species of the model are listed in Table 1.

Objective function for parameter estimation

Parameters were estimated by minimizing a modified version of a previously described objective function, U, comprising the normalized root mean square deviation (RMSD) between experimentally observed time-course data and computed model predictions (8):

$$U = \sum_{i=1}^{N_{\exp t}} \sum_{j=1}^{N_{obs}} \sum_{k=1}^{N_t} \frac{(x_{ij}(t_k) - x_{ij}^e(t_k))^2}{\sqrt[2]{((x_{ij}^e(t_k))^2)}} \tag{5}$$

where x was the concentration of some particular species in the model, x^e was the experimentally observed concentration of the same species, N_{obs} was the number of experimentally

observed species, N_{expt} was the number of experimental conditions, as defined by the relative percentage of proteins assigned to the monothiol and dithiol protein pools, and N_t was the number of time points sampled.

Sensitivity analysis

The finite difference approximation (FDM) method was used to calculate the sensitivity coefficient, $s_{i,j}$, which defined the difference between the nominal and perturbed solutions offered by the model, according to the equation (53):

$$s_{i,j}(t) = \frac{\partial x_i(t)}{\partial \theta_j} = \frac{x_i(\theta_j + \Delta \theta_j, t) - x_i(\theta_j, t)}{\Delta \theta_j} \tag{6}$$

where $x_i(\theta_j, t)$ represented a measured model output at time t, when a particular parameter had the value θ_j; subsequently, $x_i(\theta_j + \theta_j, t)$ represented the value of the same model output when the same parameter had been perturbed by the value θ_j. For the purposes of this model, all parameters were perturbed by 10% of their initial values. As a result of the difference in magnitude between parameters, the absolute sensitivity values obtained from Equation 6 were not accurate measures of relative sensitivity. To calculate the relative sensitivities for a more-direct comparison of model response at different states across different parameters, we used a normalization method previously described (53):

$$\bar{s}_{i,j}(t) = \frac{\partial x_i / x_i}{\partial \theta_j / \theta_j} \tag{7}$$

From this equation, the normalized sensitivity of a particular model output to perturbations in a particular parameter at time, t, could be determined. All sensitivity-analysis calculations were done at $t = 5$ min, and parameter sensitivities were calculated with respect to the concentrations of the experimentally determined model species (extracellular peroxide, intracellular GSH, intracellular GSSG, intracellular reduced Trx1, and intracellular oxidized Trx1).

Experimental Materials and Methods

Materials, cell culture, and stimulation conditions

All reagents were from Sigma-Aldrich, St. Louis, MO, unless specified otherwise. Jurkat cells (clone E6-1) were obtained from American Type Culture Collection (ATCC, Manassas, VA). Cells were cultured in supplemented RPMI-1640 medium (glutamine, nonessential amino acids, 100 U/ml penicillin/streptomycin, 1 mM sodium pyruvate, 10 mM HEPES, 10% FBS). For stimulation, cells were resuspended in fresh media (1×10^6 cells/ml) and treated with H_2O_2 for various times at 37°C before lysing. Pyruvate is known to undergo oxidative decarboxylation in the presence of H_2O_2, so a control experiment was performed to determine the rate of H_2O_2 removal by the culture media alone. An Amplex Red assay (Invitrogen, Carlsbad, CA) showed that the background oxidation of sodium pyruvate in the media by H_2O_2 was not detectable for the duration of the treatment conditions used throughout the study.

Cellular fractionation and derivatization of protein thiols

After treatment, cells were pelleted by centrifugation at 300 g. The cell pellet was immediately resuspended in guanidine-

Tris solution (50 mM Tris-HCL, pH 8.3, 3 mM EDTA, 6 M guanidine-HCL, 0.5% Triton X-100) supplemented with 50 mM iodoacetic acid (IAA, pH 8.3), and incubated at 37°C in the dark for 45 min (46). This procedure was carried out to lyse simultaneously the cells and derivatize reduced protein thiols. After incubation, the samples were run through Microspin G-25 columns (GE Healthcare, Buckinghamshire, U.K.) to remove excess IAA.

Redox Western blot analysis

To analyze the redox state of cytosolic Trx1, derivatized proteins were separated by native polyacrylamide gel electrophoresis, as previously described (46). PVDF membranes were probed with antibody to human Trx1 (American Diagnostica, Stamford, CT) and a goat IgG-IRDye 800 CW conjugated antibody (Rockland Immunochemicals, Gilbertsville, PA). Trx1 bands were visualized and quantified by using the LI-COR Odyssey scanner 2.1 (Lincoln, NE) and the LI-COR Odyssey 2.1 gel analysis software, respectively.

Measurement of intracellular GSH and GSSG

GSH and GSSG were measured with high-performance liquid chromatography (HPLC) as S-carboxymethyl N-dansyl derivatives by using γ-glutamylglutamate as an internal standard (18).

Calculation of E_h values

The redox potentials of GSH and Trx1 were calculated by using the Nernst equation. To convert total values for GSH and GSSG into intracellular concentrations, measured intracellular protein concentrations were used, and a constant cellular water volume (5 μl/mg protein) was assumed. The integrated band intensities of reduced and oxidized Trx1, as quantified by the LI-COR Odyssey 2.1 gel analysis software, were assumed to be directly proportional to the normalized intracellular concentrations of these species (47). The intracellular pH was assumed to be 7.4 (34) and to be unaffected by H_2O_2 treatment. E_0 values used for pH 7.4 were as follows: GSH/GSSG redox couple, -264 mV; and for the active site dithiol/disulfide of Trx1, -254 mV (46).

Results

Parameter and species fitting

Table 1 lists the kinetic parameter values obtained from the literature and the fitted values determined for the unknown parameters in the fast model. Whereas the slow model (Fig. 2A, left panel) was able to represent accurately the dynamics of peroxide consumption and the oxidation dynamics of the glutathione redox couple, it was unable to capture accurately the oxidation dynamics of the thioredoxin redox couple, Fig. 2D. The fast model (Fig. 2A, right panel), conversely, was able to capture the entire dynamic dataset. The fitted values in the fast model for the rates of protein oxidation for Pr-SH and Pr-$(SH)_2$ (k_{14} and k_{18}, respectively) were 1×10^4 M/s and 5×10^5 M/s. These values were within the order-of-magnitude range of predicted reaction rates for protein thiols with H_2O_2 (10 to 10^6 M/s) (9). Because the fast model was able to replicate better the experimental data, we used this model to generate all subsequent parameter estimates and model predictions.

The permeability constant (Equation 1) that describes the movement of peroxide through the plasma membrane, k_1, was fitted to a value of 1.0×10^{-5} cm/s. This value was approximately 1 order of magnitude smaller than the value estimated by Antunes and Cadenas (3).

Table 2 lists the initial species concentrations obtained from the literature and the fitted values determined for the concentration of protein thiols dependent on GSH and Trx1, respectively, for reduction. The protein thiol distribution that resulted in the minimization of the objective function was 42% GSH-dependent protein thiols and 58% Trx1-dependent protein thiols.

Consumption of H_2O_2 by intact Jurkat cells

The rate at which Jurkat cells clear the extracellular environment of H_2O_2 is an effective measure of their internal antioxidative response system. We fitted the model to the condition of a bolus addition of 100 μM extracellular H_2O_2 being consumed by 1×10^6 Jurkat cells per milliliter. The model-predicted rate of extracellular H_2O_2 decay was 9.4×10^{-4} per second per 10^6 cells. This decay rate was very close to the experimentally determined $1.0\pm0.1\times10^{-3}$ per second per 10^6 cells reported by Antunes and Cadenas (3).

After the model parameters and protein thiol distributions were optimized based on the bolus condition, we investigated the ability of the model to describe hydrogen peroxide consumption by Jurkat cells at varied extracellular peroxide conditions. Without any additional parameter optimization, the fitted model accurately simulated the extracellular decay of 50 μM hydrogen peroxide at a cell density of 1×10^6 cells/ml from another published dataset (13). This new peroxide concentration was 50% less than what was used in the model-fitting exercises (Fig. 3A). We also simulated the peroxide-consumption dynamics of a population of Jurkat cells exposed to low steady-state levels of extracellular H_2O_2. Because the steady-state consumption behavior of Jurkat cells was not used to fit any of the parameters contained in the model, the steady-state consumption experiment, previously carried out by Antunes and Cadenas (3), served as additional validation for the model. In this experiment, cells at a concentration of 1×10^6 cells/ml were incubated simultaneously with a low concentration of H_2O_2 and glucose oxidase to generate a steady-state extracellular H_2O_2 concentration of ~9 μM (3). The model simulation for this condition accurately predicted that Jurkat cells (1×10^6 cells/ml) would be able to maintain, at a constant level, the low concentration of H_2O_2 in their extracellular environment for ≥1 h after exposure (data not shown).

The intracellular GSH/GSSG pool is transiently oxidized by H_2O_2 treatment

We quantified glutathione disulfide (GSSG) to be $\sim0.5\%$ of the total glutathione pool in resting Jurkat cells (E_h value of cytosolic GSH/GSSG $= -230\pm3$ mV). At 5 min after H_2O_2 addition, the intracellular GSH/GSSG redox potential had been oxidized by ~8 mV (Fig. 2C). Within 30 min of treatment, the concentration of GSSG was approaching its baseline level. In contrast, the intracellular GSH concentration increased slightly; therefore, a net change in total glutathione was occurring over the experimental window of observation. At 60 min of exposure, the E_h value of the GSH/GSSG pool was -235 ± 4 mV.
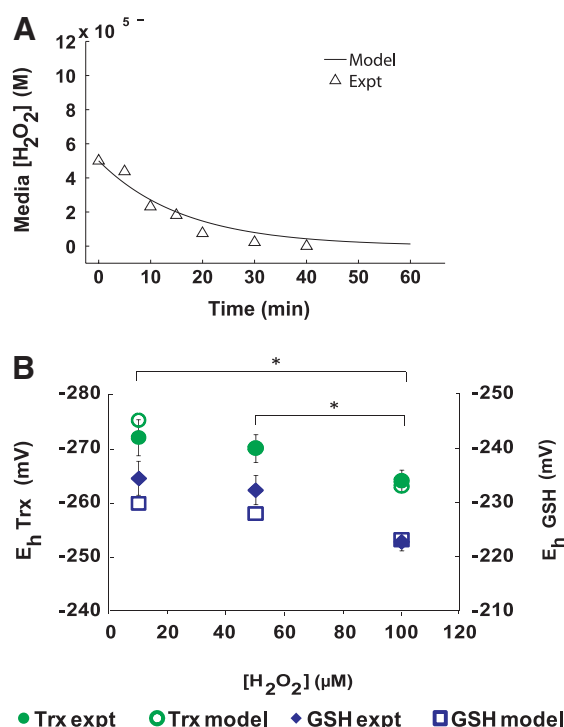
FIG. 3. Model validation for varied initial extracellular peroxide concentrations. (**A**) Model-simulated and experimentally determined (13) consumption of H_2O_2 by intact Jurkat T cells (cell density, 1×10^6 cells/ml) after being exposed to a bolus addition of $50 \mu M$ extracellular H_2O_2. (**B**) Model-simulated and experimentally determined glutathione and thioredoxin redox potentials for varying initial extracellular $[H_2O_2]$ (Jurkat T-cell density, 1×10^6 cells/ml). *Asterisks indicate statistically significant differences ($p < 0.05$) with respect to the two hydrogen peroxide concentrations being compared.

By using the measured baseline values of oxidized and reduced glutathione as initial conditions for GSH and GSSG, the model simulated the changing glutathione redox potential due to H_2O_2 treatment as a function of time (Fig. 2C). A rapid oxidation of the GSH/GSSG pool with H_2O_2 treatment resulted in an E_h value of -224 mV at 5 min after treatment, very close to the 8-mV magnitude oxidation measured. The model curve showed a return to baseline redox potential after 60 min, and, as a result of the incorporation of glutathione transport and synthesis, the model was capable of capturing the slight overshoot seen experimentally.

Cytosolic Trx1 oxidation is sustained after H_2O_2 treatment

We measured cytosolic Trx1 in resting Jurkat cells to be ~85% reduced, corresponding to an E_h value for cytosolic Trx1 of -277 ± 1.4 mV (Fig. 2D), a value that is in agreement with previous reports of the steady-state redox potential of cytosolic Trx1 (21). The potential of the Trx1 redox couple at 5 min of treatment was approximately -263 mV, reflecting 14 mV oxidation. From 5 to 30 min of treatment, the percentage of oxidized Trx1 began to decline toward its baseline value. At 60 min of treatment, however, the redox potential of

the cytosolic Trx1 redox couple was reoxidized. The 60-min Trx E_h value of -265 ± 1.6 mV was very similar to the level of Trx1 oxidation seen at 5 min of treatment (Fig. 2D).

The fitted model was capable of simulating transient E_h values for cytosolic Trx1 after exposure to $100 \mu M$ H_2O_2 (Fig. 2D). The baseline distributions of oxidized and reduced Trx1 were used as the initial conditions for the Trx1 species in the simulation. An appropriate degree of Trx1 oxidation on exposure to H_2O_2 was reproduced by the model, and the model was capable of simulating the reoxidation observed at the 60-min time point.

Model sensitivity analysis

We conducted sensitivity analysis to identify the parameters with the greatest influence on model simulation results. The parameter to which a majority of the species investigated was most sensitive was k_1, the permeability constant of the cytoplasmic membrane. Reduced and oxidized Trx1 showed the highest sensitivity to the parameters k_1, k_{12}, and k_{21}, where k_{12} and k_{21} represented the rate constant for the reduction of oxidized peroxiredoxin (Prx-SS) by reduced Trx1 and the rate constant for the reduction of oxidized Trx1 by TR and NADPH, respectively. GSH showed the highest sensitivity to k_1 and k_3, where k_3 represented the rate constant for the GPx-catalyzed reaction of GSH with hydrogen peroxide. GSSG showed the highest sensitivity to k_3 and k_{20}, where k_{20} represented the reduction of GSSG by GR and NADPH. Although both the glutathione and thioredoxin redox couples showed relatively high sensitivity to k_{22}, the rate constant describing the rate of NADPH resupply by the G6PDH enzyme, the Trx redox couple was more sensitive to perturbations in this parameter than was the GSH redox couple. Model components, in general, were "insular" in their sensitivities (*i.e.*, affected by rate constants of reactions in which they played either a direct or very nearly direct role), with very few enzymatic parameters, such as k_{22} (NADPH supply), affecting both the thioredoxin and glutathione couples.

Model predicts oxidation profiles of glutathione and thioredoxin redox couples for varied initial extracellular $[H_2O_2]$

The antioxidative properties of our model were capable of replicating *in vivo* Jurkat dynamics for particular instances of both the transient and steady-state condition of oxidative stress. To interrogate the system further, we explored the model's ability to predict these dynamic responses for a variety of oxidation levels. We simulated a bolus extracellular H_2O_2 addition of $10 \mu M$ and $50 \mu M$ at a cell density of 1×10^6 cells/ml and compared the results with the redox potential of the glutathione and thioredoxin redox couples experimentally measured 5 min after treatment (Fig. 3B). Significant statistical differences (alpha = 0.05) were found between the experimentally determined redox potentials of the glutathione and thioredoxin redox couples at 5 min of $10 \mu M$ peroxide treatment compared with the $100 \mu M$ peroxide treatment. Statistically significant differences were also seen between the $50 \mu M$ and the $100 \mu M$ extracellular peroxide treatments. Model simulations of the redox potential of the glutathione and thioredoxin redox couples for the $10 \mu M$, $50 \mu M$, and $100 \mu M$ peroxide treatments deviated slightly from the experimental values but accurately captured the

oxidative change between the redox potentials of both redox couples for all peroxide treatment conditions examined (Fig. 3B).

Model predicts intracellular peroxide concentrations and levels of protein thiol oxidation resulting from exogenous hydrogen peroxide

One benefit of the model is the ability to offer quantitative estimates for the intracellular [H_2O_2] resulting from an external source of hydrogen peroxide. The model predicts that a concentration of about $8 \times 10^{-8}\,M$ of hydrogen peroxide develops within the cell when it is exposed to $100\,\mu M$ extracellular peroxide at a cell density of 1×10^6 cells/ml (Fig. 4), thereby representing a gradient of $\sim 1,000$ that develops between the extracellular environment and the intracellular cytosol.

In addition to offering quantitative estimates of the intracellular peroxide concentration, the model is capable of providing predictions of protein thiol oxidation. The protein thiol pool may significantly contribute to the cellular antioxidant defense because of the substantial concentration of protein thiols in the cell (19). To investigate the independent roles of mono- and dithiol proteins during dynamic oxidative conditions, we used the model to predict the level of peroxide-induced protein oxidation as a function of initial extracellular [H_2O_2] (Fig. 5). For this *in silico* experiment, protein oxidation was quantified by the concentration of protein disulfides ([P-SS-P]) and *S*-glutathione adducts ([P-SSG]) observed at 5 min of $100\,\mu M$ H_2O_2 treatment for the slow and the fast model of peroxide consumption. The slow model, which was unable to fit all the experimental data (Fig. 2), showed very little protein oxidation, with the maximum concentration of protein

S-glutathione adducts and protein disulfides not exceeding 1% of the total thiol pool (Fig. 5, top). Conversely, the fast model, which was capable of fitting all the experimental data, predicted a significant increase in the concentration of protein disulfides, $\sim 10\%$ of the total protein thiol pool (Fig. 5, bottom).

Discussion

The development of kinetic computational models of redox enzyme systems presents unique challenges in comparison with other biochemical networks. The nonequilibrium condition of intracellular thiol-based redox couples provides a rapid and highly sensitive switching mechanism in response to changes in intracellular redox state (21). Because many thiol-based redox couples are set at different potentials, the model species tend to equilibrate even in the absence of oxidative stress. The spontaneous change in redox potential that is due to this inherent nonequilibrium condition must be filtered out to focus entirely on those changes that are the result of oxidative stress alone. One modeling approach is to define the driving force for electron transfer to be the function of the difference between the homeostatic potential and the actual potential of the system, as defined by the redox couple of interest (21). With this approach, the defined system can describe the dynamic response to changes in intracellular [H_2O_2] without having explicitly to include the numerous
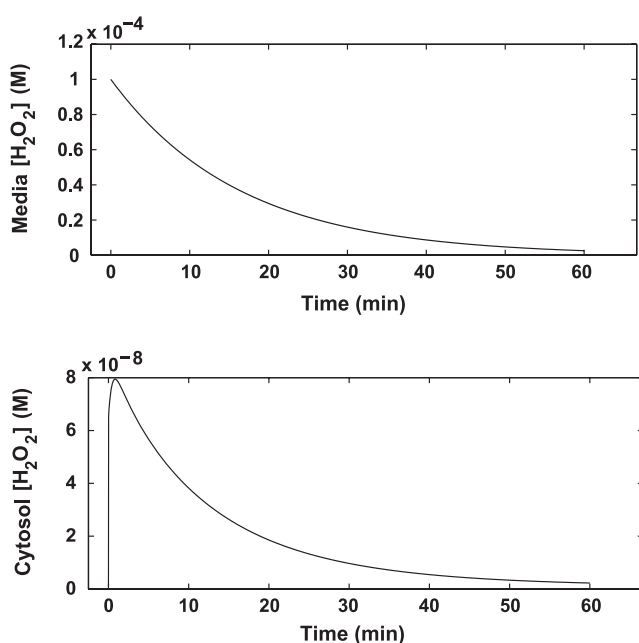

FIG. 4. Model-predicted intracellular [H_2O_2]. Dynamic model-simulated extra- (*top*) and intracellular (*bottom*) peroxide concentration as a result of $100\,\mu M$ H_2O_2. (Jurkat T-cell density $= 1 \times 10^6$ cells/ml).
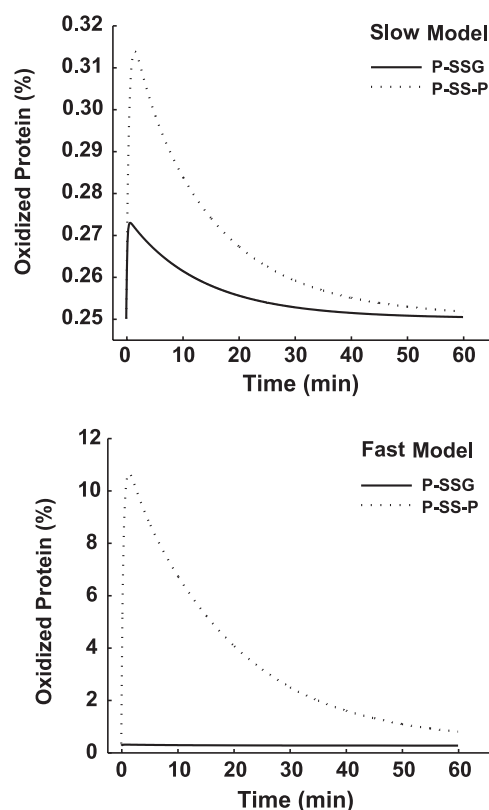

FIG. 5. Model-predicted protein-oxidation profiles. Simulated percentages of *S*-glutathionylated proteins and protein disulfides that form as a result of oxidative stress ($100\,\mu M$ H_2O_2; Jurkat T-cell density $= 1 \times 10^6$ cells/ml) for the slow (*top*) and fast (*bottom*) models.

steady-state fluxes that must occur across cellular membranes to maintain the redox couples out of equilibrium.

Importance of membrane permeability in cellular antioxidant defense

The model highlights the sensitivity of the entire redox enzyme network to the membrane permeability constant for hydrogen peroxide and revises estimates for this constant. The first barrier to extracellular hydrogen peroxide consumption is the cytoplasmic membrane. Transmembrane diffusion of H_2O_2 is an important factor in the maintenance of peroxide gradients between the extracellular environment and the intracellular cytosol (5). The model recapitulated this experimental observation by highlighting k_1, the model parameter describing the permeability coefficient of the cytoplasmic membrane, as the parameter to which most model components were the most sensitive. The optimized permeability coefficient was approximately 1 order of magnitude smaller than that previously estimated by Antunes and Cadenas (3). The literature-reported estimate calculated by Antunes and Cadenas was based on the assumption that the GPx and catalase pathways were the only pathways working toward H_2O_2 removal. Realistically, however, the cell has several additional enzymatic and nonenzymatic methods of H_2O_2 clearance, most of which have been integrated into this present model. Without the incorporation of all redox reactions that take place *in vivo*, an overestimated value for the permeability coefficient is expected. From a systems perspective, therefore, it would be beneficial if the cell could control its cytoplasmic membrane permeability to control the amount of transmembrane H_2O_2 diffusion it experiences. Recent studies have shown that some membranes are poorly permeable to H_2O_2, compared with other membranes, implying that transport of H_2O_2 could be regulated (5). Differences in membrane permeability could be attributed to changes in membrane lipid composition or changes in the number of membrane-bound diffusion-facilitating channel proteins, all of which can be controlled by the cell. The importance of the membrane-permeability coefficient, as dictated by the model-sensitivity analysis, suggested that the cytoplasmic membrane permeability is a parameter capable of being tuned by the cell to control H_2O_2 transport and, ultimately, the concentration of H_2O_2 inside the cell. Whether such transport could be actively controlled by aquaporins is presently unknown.

Precise modeling of the intracellular peroxide consumption dynamics and membrane permeability provides a more-accurate description of intracellular peroxide levels. The model-predicted peak intracellular concentration of hydrogen peroxide that is induced by $100\,\mu M$ is about $100\,nM$. The model is the most comprehensive model to date to offer quantitative and dynamic estimates of the intracellular concentration of hydrogen peroxide resulting from external peroxide assault.

Unequal antioxidative burden of intracellular redox enzymes and thiol-containing compounds

The model addresses which redox enzymes and thiol-containing compounds are primarily responsible for the antioxidant capacity of the cell. The Trx1 and GSH redox couples are often used as measures of the overall redox state of the cell (41). We used the model to describe the dynamics of these two

redox couples under conditions of oxidative stress. Experimental results showed the E_h value of the Trx1 redox couple to be oxidized by a maximum of $17\,mV$ after treatment with $100\,\mu M$ H_2O_2. This maximum level of oxidation was about twice as high as that seen for the GSH redox couple. Analysis of the model system under the steady-state peroxide-generation condition (Table 3) suggested that an unequal distribution of the antioxidative burden exists between the Trx1 and GSH redox couples in the intracellular cytosol; this unequal distribution offers one explanation for the unequal oxidation of the Trx1 and GSH redox couples described earlier. These results should be interpreted carefully, as the flux distribution between the Trx1 and GSH redox couples may very well be compartment specific and therefore altered in other subcellular compartments. Furthermore, Trx1 kinetics may change with hyperoxidation of the enzyme (46), and the kinetics of the G6PD enzyme are altered as a result of increasing levels of GSSG in the cell (45). Future modeling efforts may need to account for these complex kinetic regulatory mechanisms to simulate more extreme oxidative conditions appropriately.

The steady-state concentration of H_2O_2 that develops within an individual cell as a result of a low ($\sim 9\,\mu M$), constant level of extracellular H_2O_2 was $\sim 1\,nM$ (data not shown). From this steady-state value, and using the respective rate constants of peroxide metabolism for each antioxidative branch [catalase, GPx/GSH, Prx/Trx1, Pr-SH, Pr-(SH)$_2$], in addition to the relative concentrations of the species in each branch, we were able to calculate the hydrogen peroxide flux (M/s) that passes through each antioxidative branch (Table 3). These calculations revealed that the GPx and Prx enzyme systems were responsible for the majority of the peroxide metabolism at this steady-state condition, with calculated fluxes of $6.0\times10^{-6}\,M/s$ and $4.4\times10^{-6}\,M/s$, respectively. In comparison, the flux through the catalase enzyme system was only $3.7\times10^{-8}\,M/s$, approximately 0.6% of the flux through the GPx enzyme system. The contribution of catalase to the consumption of externally generated hydrogen peroxide is low compared with other antioxidant enzymes such as peroxiredoxin and glutathione peroxidase. This result reflects not only the low peroxisomal content of Jurkat cells, but also the inefficiency of intact peroxisomes in degrading externally generated hydrogen peroxide (10). It must be noted that although catalase may be somewhat inefficient at degrading external hydrogen peroxide, it is highly efficient at degrading hydrogen peroxide generated within the peroxisomal matrix.

Another prediction by the model flux analysis was the contribution of the protein dithiol pool to the steady-state peroxide consumption. The flux of hydrogen peroxide through the protein dithiol pool was $3.1\times10^{-6}\,M/s$, $\sim 23\%$ of

TABLE 3. STEADY STATE HYDROGEN PEROXIDE FLUXES

Branch	Flux (M/s)	Flux (% of total)	Flux (M/s)	Flux (% of total)
Prx	4.4×10^{-6}	32	5.6×10^{-6}	42
GPx	6.0×10^{-6}	44	7.7×10^{-6}	57
Catalase	3.7×10^{-8}	<1	4.6×10^{-8}	<1
Pr-SH	7.0×10^{-9}	<1	1.1×10^{-8}	<1
Pr-(SH)$_2$	3.1×10^{-6}	23	1.1×10^{-8}	<1
	Fast model		Slow model	

the total hydrogen peroxide consumption within the cell. Comparatively, the flux through the protein monothiol pool was <1%. These results are in line with previous predictions of protein thiol oxidation that suggest that a majority of the proteins in the cell react at relatively slow rates with hydrogen peroxide, whereas a few proteins, primarily those that form disulfide bonds, react with hydrogen peroxide at appreciably faster rates (49, 50). This result offers another possible explanation for the thioredoxin redox couple experiencing more pronounced and sustained oxidation during times of oxidative stress as compared with its glutathione counterpart.

The current model advances our understanding of intracellular redox biology

Multiple advances in knowledge have been gained by this modeling study. We asked whether the current knowledge in the redox biology field can explain experimental data, or if additional redox nodes, which have not yet been discovered, may significantly contribute to peroxide clearance from the intracellular environment. We have shown that the model topology, as it currently stands and with current parameter measurements available in the literature, is capable of describing the behavior of a particular cell line on exposure to an external source of hydrogen peroxide if supplemented with the optimized estimates of unknown parameters. Although customized for Jurkat cells, the reactions that are described by the model can easily be adapted to other cell lines by inserting enzyme concentrations and reaction rate constants for the particular cell line of interest. The second contribution given by this model is its ability to provide predictions of the oxidation profiles of specific intracellular components that we cannot yet quantify experimentally. The current model offers what we believe is the first fully quantitative estimate for the concentration of intracellular hydrogen peroxide that results from an extracellular source, in addition to the percentage of protein thiols that undergo both protein S-glutathionylation and protein disulfide formation. By including the contribution of the protein thiols to hydrogen peroxide clearance, the model explains why the glutathione and thioredoxin redox potentials are purported to be independent of one another; the larger flux through the dithiol pool causes a capacitance in the thioredoxin branch that leads to a sustained oxidation of thioredoxin.

Finally, the model is capable of simultaneously determining relative fluxes through each antioxidant branch, which would be extremely difficult to measure by using traditional experimentation.

This framework used carefully controlled induction of oxidative stress to construct a kinetic model that is capable of describing the observed oxidation of redox couples as a function of time. As a tool for interrogation of a particular biochemical network, a bolus condition is extremely useful to "reverse-engineer" features. Although the current model was fitted and validated with data based on the extracellular administration of hydrogen peroxide, this does not negate the ability of the model to simulate and predict the behavior of intracellular components as a result of endogenous generation of hydrogen peroxide. To validate these dynamics, however, advancements in the ability to measure quantitatively the intracellular peroxide must be developed. Furthermore, although compartmentation was included, spatial gradients within the cell were not described by this model. With the

network structure and kinetic description intact, future challenges to modeling efforts will involve the added complexity of intracellular H_2O_2 spatial gradients generated by NADPH oxidases, peroxisomes, and mitochondria.

Author Disclosure Statement

No competing financial interests exist.

References

1. Aebi H. Catalase in vitro. *Methods Enzymol* 105: 121–126, 1984.
2. Akerboom TP, Bilzer M, and Sies H. The relationship of biliary glutathione disulfide efflux and intracellular glutathione disulfide content in perfused rat liver. *J Biol Chem* 257: 4248–4252, 1982.
3. Antunes F and Cadenas E. Estimation of H_2O_2 gradients across biomembranes. *FEBS Lett* 475: 121–126, 2000.
4. Arner ES, Zhong L, and Holmgren A. Preparation and assay of mammalian thioredoxin and thioredoxin reductase. *Methods Enzymol* 300: 226–239, 1999.
5. Bienert GP, Schjoerring JK, and Jahn TP. Membrane transport of hydrogen peroxide. *Biochim Biophys Acta* 1758: 994–1003, 2006.
6. Chae HZ, Kim HJ, Kang SW, and Rhee SG. Characterization of three isoforms of mammalian peroxiredoxin that reduce peroxides in the presence of thioredoxin. *Diabetes Res Clin Pract* 45: 101–112, 1999.
7. Chang TS, Jeong W, Woo HA, Lee SM, Park S, and Rhee SG. Characterization of mammalian sulfiredoxin and its reactivation of hyperoxidized peroxiredoxin through reduction of cysteine sulfinic acid in the active site to cysteine. *J Biol Chem* 279: 50994–51001, 2004.
8. Chen WW, Schoeberl B, Jasper PJ, Niepel M, Nielsen UB, Lauffenburger DA, and Sorger PK. Input-output behavior of ErbB signaling pathways as revealed by a mass action model trained against dynamic data. *Mol Syst Biol* 5: 239, 2009.
9. D'Autreaux B and Toledano MB. ROS as signalling molecules: mechanisms that generate specificity in ROS homeostasis. *Nat Rev Mol Cell Biol* 8: 813–824, 2007.
10. Fritz R, Bol J, Hebling U, Angermuller S, Volkl A, Fahimi HD, and Mueller S. Compartment-dependent management of H(2)O(2) by peroxisomes. *Free Radic Biol Med* 42: 1119–1129, 2007.
11. Gallogly MM and Mieyal JJ. Mechanisms of reversible protein glutathionylation in redox signaling and oxidative stress. *Curr Opin Pharmacol* 7: 381–391, 2007.
12. Gilbert HF. Molecular and cellular aspects of thiol-disulfide exchange. *Adv Enzymol Relat Areas Mol Biol* 63: 69–172, 1990.
13. Hampton MB and Orrenius S. Dual regulation of caspase activity by hydrogen peroxide: implications for apoptosis. *FEBS Lett* 414: 552–556, 1997.

14. Hansen JM, Go YM, and Jones DP. Nuclear and mitochondrial compartmentation of oxidative stress and redox signaling. *Annu Rev Pharmacol Toxicol* 46: 215–234, 2006.

15. Henderson GB, Murgolo NJ, Kuriyan J, Osapay K, Kominos D, Berry A, Scrutton NS, Hinchliffe NW, Perham RN, and Cerami A. Engineering the substrate specificity of glutathione reductase toward that of trypanothione reduction. *Proc Natl Acad Sci U S A* 88: 8769–8773, 1991.

16. Holmgren A. Thioredoxin. *Annu Rev Biochem* 54: 237–271, 1985.

17. Ishizuka M, Toyama Y, Watanabe H, Fujiki Y, Takeuchi A, Yamasaki S, Yuasa S, Miyazaki M, Nakajima N, Taki S, and Saito T. Overexpression of human acyl-CoA thioesterase upregulates peroxisome biogenesis. *Exp Cell Res* 297: 127–141, 2004.

18. Jones DP. Redox potential of GSH/GSSG couple: assay and biological significance. *Methods Enzymol* 348: 93–112, 2002.

19. Jones DP. Radical-free biology of oxidative stress. *Am J Physiol Cell Physiol* 295: 849–868, 2008.

20. Jones DP, Go YM, Anderson CL, Ziegler TR, Kinkade JM Jr, and Kirlin WG. Cysteine/cystine couple is a newly recognized node in the circuitry for biologic redox signaling and control. *FASEB J* 18: 1246–1248, 2004.

21. Kemp M, Go YM, and Jones DP. Nonequilibrium thermodynamics of thiol/disulfide redox systems: a perspective on redox systems biology. *Free Radic Biol Med* 44: 921–937, 2008.

22. Kondo N, Ishii Y, Kwon YW, Tanito M, Horita H, Nishinaka Y, Nakamura H, and Yodoi J. Redox-sensing release of human thioredoxin from T lymphocytes with negative feedback loops. *J Immunol* 172: 442–448, 2004.

23. Lee TK, Hammond CL, and Ballatori N. Intracellular glutathione regulates taurocholate transport in HepG2 cells. *Toxicol Appl Pharmacol* 174: 207–215, 2001.

24. Liu H, Colavitti R, Rovira II, and Finkel T. Redox-dependent transcriptional regulation. *Circ Res* 97: 967–974, 2005.

25. Lo HW, Antoun GR, and Ali-Osman F. The human glutathione S-transferase P1 protein is phosphorylated and its metabolic function enhanced by the Ser/Thr protein kinases, cAMP-dependent protein kinase and protein kinase C, in glioblastoma cells. *Cancer Res* 64: 9131–9138, 2004.

26. Low FM, Hampton MB, Peskin AV, and Winterbourn CC. Peroxiredoxin 2 functions as a noncatalytic scavenger of low-level hydrogen peroxide in the erythrocyte. *Blood* 109: 2611–2617, 2007.

27. Lundberg M, Fernandes AP, Kumar S, and Holmgren A. Cellular and plasma levels of human glutaredoxin 1 and 2 detected by sensitive ELISA systems. *Biochem Biophys Res Commun* 319: 801–809, 2004.

28. Makino N, Sasaki K, Hashida K, and Sakakura Y. A metabolic model describing the H2O2 elimination by mammalian cells including H2O2 permeation through cytoplasmic and peroxisomal membranes: comparison with experimental data. *Biochim Biophys Acta* 1673: 149–159, 2004.

29. Manta B, Hugo M, Ortiz C, Ferrer-Sueta G, Trujillo M, and Denicola A. The peroxidase and peroxynitrite reductase activity of human erythrocyte peroxiredoxin 2. *Arch Biochem Biophys* 484: 146–154, 2009.

30. Martinovich G, Cherenkevich S, and Sauer H. Intracellular redox state: towards quantitative description. *Eur Biophys J* 34: 937–942, 2005.

31. Moore RB, Mankad MV, Shriver SK, Mankad VN, and Plishker GA. Reconstitution of Ca(2+)-dependent K+ transport in erythrocyte membrane vesicles requires a cytoplasmic protein. *J Biol Chem* 266: 18964–18968, 1991.

32. Mueller S, Riedel HD, and Stremmel W. Determination of catalase activity at physiological hydrogen peroxide concentrations. *Anal Biochem* 245: 55–60, 1997.

33. Ng CF, Schafer FQ, Buettner GR, and Rodgers VG. The rate of cellular hydrogen peroxide removal shows dependency on GSH: mathematical insight into in vivo H2O2 and GPx concentrations. *Free Radic Res* 41: 1201–1211, 2007.

34. Nordstrom T, Mustelin T, Pessa-Morikawa T, and Andersson LC. Modulation of calcium fluxes in Jurkat T cells by myristic acid: inhibition is independent of membrane potential and intracellular pH. *Biochem J* 283(Pt 1): 113–118, 1992.

35. Oliveira-Marques V, Marinho HS, Cyrne L, andAntunes F. Role of hydrogen peroxide in NF-kappaB activation: from inducer to modulator. *Antioxid Redox Signal* 11: 2223–2243, 2009.

36. Peltoniemi MJ, Karala AR, Jurvansuu JK, Kinnula VL, and Ruddock LW. Insights into deglutathionylation reactions: different intermediates in the glutaredoxin and protein disulfide isomerase catalyzed reactions are defined by the gamma-linkage present in glutathione. *J Biol Chem* 281: 33107–33114, 2006.

37. Peskin AV, Low FM, Paton LN, Maghzal GJ, Hampton MB, and Winterbourn CC. The high reactivity of peroxiredoxin 2 with H(2)O(2) is not reflected in its reaction with other oxidants and thiol reagents. *J Biol Chem* 282: 11885–11892, 2007.

38. Poole B. Diffusion effects in the metabolism of hydrogen peroxide by rat liver peroxisomes. *J Theor Biol* 51: 149–167, 1975.

39. Rhee SG, Kang SW, Chang TS, Jeong W, and Kim K. Peroxiredoxin, a novel family of peroxidases. *IUBMB Life* 52: 35–41, 2001.

40. Sasaki K, Bannai S, and Makino N. Kinetics of hydrogen peroxide elimination by human umbilical vein endothelial cells in culture. *Biochim Biophys Acta* 1380: 275–288, 1998.

41. Schafer FQ and Buettner GR. Redox environment of the cell as viewed through the redox state of the glutathione disulfide/glutathione couple. *Free Radic Biol Med* 30: 1191–1212, 2001.

42. Seaver LC and Imlay JA. Hydrogen peroxide fluxes and compartmentalization inside growing *Escherichia coli*. *J Bacteriol* 183: 7182–7189, 2001.

43. Srinivasan U, Mieyal PA, and Mieyal JJ. pH profiles indicative of rate-limiting nucleophilic displacement in thiol-transferase catalysis. *Biochemistry* 36: 3199–3206, 1997.

44. Trujillo M, Clippe A, Manta B, Ferrer-Sueta G, Smeets A, Declercq JP, Knoops B, and Radi R. Pre-steady state kinetic characterization of human peroxiredoxin 5: taking advantage of Trp84 fluorescence increase upon oxidation. *Arch Biochem Biophys* 467: 95–106, 2007.

45. Ursini MV, Parrella A, Rosa G, Salzano S, and Martini G. Enhanced expression of glucose-6-phosphate dehydrogenase in human cells sustaining oxidative stress. *Biochem J* 323(Pt 3): 801–806, 1997.

46. Watson WH and Jones DP. Oxidation of nuclear thioredoxin during oxidative stress. *FEBS Lett* 543: 144–147, 2003.

47. Watson WH, Pohl J, Montfort WR, Stuchlik O, Reed MS, Powis G, and Jones DP. Redox potential of human thioredoxin 1 and identification of a second dithiol/disulfide motif. *J Biol Chem* 278: 33408–33415, 2003.

48. Watson WH, Yang X, Choi YE, Jones DP, and Kehrer JP. Thioredoxin and its role in toxicology. *Toxicol Sci* 78: 3–14, 2004.

49. Winterbourn CC and Hampton MB. Thiol chemistry and specificity in redox signaling. *Free Radic Biol Med* 45: 549–561, 2008.

50. Winterbourn CC and Metodiewa D. Reactivity of biologically important thiol compounds with superoxide and hydrogen peroxide. *Free Radic Biol Med* 27: 322–328, 1999.

51. Yang KS, Kang SW, Woo HA, Hwang SC, Chae HZ, Kim K, and Rhee SG. Inactivation of human peroxiredoxin I during catalysis as the result of the oxidation of the catalytic site cysteine to cysteine-sulfinic acid. *J Biol Chem* 277: 38029–38036, 2002.

52. Yeh GC, Occhipinti SJ, Cowan KH, Chabner BA, and Myers CE. Adriamycin resistance in human tumor cells associated with marked alteration in the regulation of the hexose monophosphate shunt and its response to oxidant stress. *Cancer Res* 47: 5994–5999, 1987.

53. Yue H, Brown M, Knowles J, Wang H, Broomhead DS, and Kell DB. Insights into the behaviour of systems biology models from dynamic sensitivity and identifiability analysis: a case study of an NF-kappaB signalling pathway. *Mol Biosyst* 2: 640–649, 2006.

Address correspondence to:
Melissa L. Kemp
Room 1314
315 Ferst Drive
Atlanta, GA 30332-0363

E-mail: melissa.kemp@bme.gatech.edu

Abbreviations Used

Cys = cysteine
GPx = glutathione peroxidase
GR = glutathione reductase
GSH = glutathione
GSSG = glutathione disulfide
H_2O_2 = hydrogen peroxide
Pr-SH = reduced protein thiol
Pr-(SH)$_2$ = reduced protein dithiol
Pr-SOH = protein sulfenic acid
Prx = peroxiredoxin
P-SSG = *S*-glutathionylated protein
P-SS-P = protein disulfide
ROS = reactive oxygen species
TR = thioredoxin reductase
Trx = thioredoxin